Available online at www.sciencedirect.com
SCIENCE DIRECT®
Thermochimica Acta 416 (2004) 93–98
thermochimica acta
www.elsevier.com/locate/tca

Thermodynamic properties of negative thermal expansion materials ZrW_2O_8 substituted for Zr site

Toshihide Tsuji [a,*], Yasuhisa Yamamura [b], Noriyuki Nakajima [a]

[a] School of Materials Science, Japan Advanced Institute of Science and Technology, 1-1 Asahidai, Tatsunokuchi, Ishikawa 923-1292, Japan
[b] Center for Nano Materials and Technology, Japan Advanced Institute of Science and Technology, 1-1 Asahidai, Tatsunokuchi, Ishikawa 923-1292, Japan

Received 30 November 2002; received in revised form 15 January 2003; accepted 24 January 2003

Available online 1 February 2004

Abstract

Thermodynamic properties of negative thermal expansion materials, ZrW_2O_8 substituted for Zr site, were studied by X-ray diffraction and heat capacity measurements. Effect of substituted ions on lattice parameters of these materials was discussed from the viewpoint of ionic radius of substituted and host ions, and of oxygen defect. The entropy of α-to-β phase transition in $Zr_{1-x}Hf_xW_2O_8$ series ($x = 0$, 0.5 and 1) was the same value of 2.1 J K^{-1} mol^{-1}. The normalized 3 1 0 diffraction peaks in $Zr_{1-x}Hf_xW_2O_8$ ($x = 0$ and 0.5) and $Zr_{0.98}Sc_{0.02}W_2O_{8-y}$, as an indicator of the order parameter, followed the universal curve against $(T - T_{trs})/T_{trs}$, where T_{trs} is the transition temperature. These results suggest that these materials have the same order–disorder phase transition mechanism. The abrupt decrease in transition temperatures of $Zr_{1-x}M_xW_2O_{8-y}$ (M = Sc, In and Y), compared to that of $Zr_{1-x}Hf_xW_2O_8$, can be explained by the decrease of ordering in α-phase due to oxygen defect.

Keywords: Negative thermal expansion; Scandium-doped ZrW_2O_8; Heat capacity; Order–disorder phase transition; Indium-doped ZrW_2O_8

1. Introduction

Many materials usually show a positive thermal expansion with increasing temperature, but there exists some of materials having a negative thermal expansion. Among them zirconium tungsten oxide, ZrW_2O_8, is one of the interesting materials, because this compound has an isotropic crystal structure with a negative thermal expansion over a wide temperature range from 4 to 1050 K [1–3]. The crystal structure of ZrW_2O_8 has a framework structure that is characterized by linkages of the corner-shared WO_4 tetrahedra and ZrO_6 octahedra. The ZrO_6 octahedral units share all corners with six WO_4 tetrahedral units, whereas each WO_4 unit shares only three of its four oxygen atoms with the adjacent ZrO_6 units. One of four oxygen atoms has, therefore, an unshared vertex of the WO_4 tetrahedron. The framework structure and the libration of the WO_4 and ZrO_6 polyhedral units result in the nature of negative thermal expansion. ZrW_2O_8 undergoes a structural phase transition at about 430 K from an acentric (α-phase, $P2_13$) to a centric structure (β-phase,$Pa\bar{3}$) with increasing temperature. The structural phase transition is of order–disorder-type related to the orientation of the unshared vertex of WO_4 unit [1–5].

It is known that the ZrW_2O_8 forms a complete solid solution with HfW_2O_8 and $ZrMo_2O_8$ [6–9]. Lattice parameters of $Zr_{1-x}Hf_xW_2O_8$ [6,7] and $ZrW_{2-x}Mo_xO_8$ [8,9] substituted by the same valence decreased with substituted content, due to smaller ionic radius of substituted ion than host lattice. An anomalous lattice constant of $Zr_{1-x}Hf_xW_2O_8$ ($x =$ 0, 0.5 and 1) and $ZrW_{2-x}Mo_xO_8$ as a function of temperature was observed around at 450 and 270 K, respectively, by X-ray diffraction method. $Zr_{1-x}Hf_xW_2O_8$ ($x = 0$, 0.5 and 1) showed an anomalous peak in heat capacity around 440–460 K by heat capacity measurement, and α-to-β structural phase transition temperature in $Zr_{1-x}Hf_xW_2O_8$ increased slightly with increasing substituted content [5,7,10].

In this paper, we synthesize $Zr_{1-x}M_xW_2O_{8-y}$ solid solutions substituted for Zr^{4+} site by Hf^{4+}, Sc^{3+}, In^{3+} and Y^{3+}, and report the effects of ionic valence, ionic radius and substituted content on the lattice parameters of $Zr_{1-x}M_xW_2O_{8-y}$ solid solutions and on

* Corresponding author.

0040-6031/$ – see front matter © 2003 Elsevier B.V. All rights reserved.
doi:10.1016/j.tca.2003.04.001

their thermodynamic properties of phase transition. Lattice parameters and phase transition temperatures of $Zr_{1-x}M_xW_2O_{8-y}$ solid solutions are compared to those of $ZrW_{2-x}Mo_xO_8$.

2. Experimental

2.1. Sample preparation and characterization

$Zr_{1-x}Sc_xW_2O_{8-y}$ ($x = 0$–0.04), $Zr_{0.96}M_{0.04}W_2O_{8-y}$ (M = In and Y) and $Zr_{1-x}Hf_xW_2O_8$ ($x = 0$–1) solid solutions were synthesized by a conventional solid-state reaction. Starting materials were ZrO_2, Sc_2O_3, In_2O_3, Y_2O_3, HfO_2 and WO_3 with high purity. These materials were thoroughly mixed at the required proportion in an agate mortar and pressed in a steel die to form pellet. The pellets were then calcined at 1473 K for 12 h in air and rapidly cooled down to room temperature. After grinding the quenched pellets to get homogeneous solid solution, the resulting powders were pressed into pellets. The pellets were sintered at 1473 K for 12 h and quenched in liquid nitrogen to avoid decomposition of solid solution.

The samples of $Zr_{1-x}Sc_xW_2O_{8-y}$ ($x = 0$–0.04), $Zr_{0.96}M_{0.04}W_2O_{8-y}$ (M = In and Y) and $Zr_{1-x}Hf_xW_2O_8$ ($x = 0$–1) were characterized by X-ray powder diffraction (XRD) method, using Cu Kα radiation with 40 kV/200 mA (RINT 2500, Rigaku). The XRD data were collected with a step width of 0.01 and a scan time of 0.7 s in the 2θ range from 10° to 100° by a step scanning method. XRD equipment has a low and intermediate temperature attachment capable of controlling temperature within ±1 K. The powder XRD patterns of the samples were obtained in a vacuum environment at about 35 temperatures from 90 to 560 K, at which temperature was kept constant at each temperature.

2.2. Heat capacity measurement

The heat capacity of $Zr_{1-x}Hf_xW_2O_8$ ($x = 0$, 0.5 and 1) was measured by an adiabatic scanning calorimeter (ASC) at temperatures from 340 to 550 K. Details of the apparatus and the operation of ASC have been described elsewhere [11,12]. Each crushed sample of $Zr_{1-x}Hf_xW_2O_8$ ($x = 0$, 0.5 and 1) was loaded into a quartz ampoule as a calorimeter vessel and sealed with small amounts of helium gas (20 kPa at room temperature) to assist thermal equilibration within the ampoule. The amount of the sample used for the measurement was about 16 g. Before heat capacity measurement was carried out, the ampoule with the sample was annealed at about 800 K for 1 h in order to remove the quenching effect in the sample preparation. The heating rate (scanning rate) chosen in this study was about 1.8 K min^{-1}. A preliminary heat capacity measurement of sapphire using ASC showed that a precision and an accuracy of the calorimeter were within ±2 and ±2%, respectively, in comparison with the reliable data of sapphire [13].

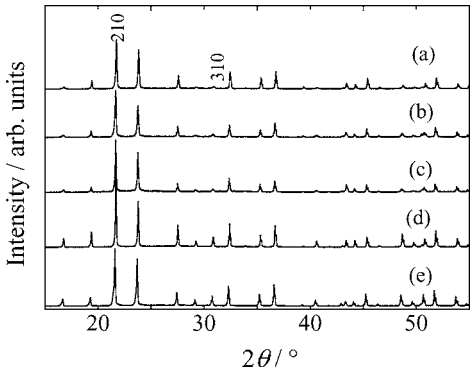

Fig. 1. XRD profiles of (a) α-$Zr_{0.96}Sc_{0.04}W_2O_{8-y}$, (b) α-$Zr_{0.96}In_{0.04}W_2O_{8-y}$, (c) α-$Zr_{0.96}Y_{0.04}W_2O_{8-y}$, (d) α-$Zr_{0.5}Hf_{0.5}W_2O_8$ and (e) α-ZrW_2O_8.

3. Results and discussion

3.1. Lattice parameter

Fig. 1 shows the XRD profiles of α-$Zr_{0.96}M_{0.04}W_2O_{8-y}$ (M = Sc, In and Y) and α-$Zr_{1-x}Hf_xW_2O_8$ ($x = 0$ and 0.5) solid solutions at 121 K. The XRD profiles of α-$Zr_{0.96}M_{0.04}W_2O_{8-y}$ (M = Sc, In and Y) and α-$Zr_{0.5}Hf_{0.5}W_2O_8$ solid solutions are very similar to that of α-ZrW_2O_8. All samples of $Zr_{1-x}Sc_xW_2O_{8-y}$ ($x = 0$–0.04), $Zr_{0.96}M_{0.04}W_2O_{8-y}$ (M = In and Y) and $Zr_{1-x}Hf_xW_2O_8$ ($x = 0$–1) solid solutions prepared were characterized to be a single phase having a cubic crystal structure by a powder XRD method. The diffraction peaks in the X-ray profiles in Fig. 1 were assigned by referring to the previous work on ZrW_2O_8 by Sleight and coworkers [2]. We express the peak intensities of the 2 1 0 and 3 1 0 shown in Fig. 1 as I_{210} and I_{310}, respectively. The I_{310}/I_{210} ratios of α-$Zr_{0.96}M_{0.04}W_2O_{8-y}$ (M = Sc, In and Y) substituted for Zr(IV) site by lower valence of M(III) are about half of that of α-ZrW_2O_8, but the I_{310}/I_{210} ratio of α-$Zr_{0.5}Hf_{0.5}W_2O_8$ substituted by the same valence of Hf(IV) is nearly the same as that of α-ZrW_2O_8. The 3 1 0 peak of all samples shown in Fig. 1 disappeared above phase transition temperature as will be shown in Fig. 3. It is thus expected that phase transition temperatures of $Zr_{0.96}M_{0.04}W_2O_{8-y}$ (M = Sc, In and Y) are lower than those of $Zr_{0.5}Hf_{0.5}W_2O_8$ and ZrW_2O_8, as will be shown in Fig. 7.

Lattice parameters of all samples prepared were determined using about 40 diffraction peaks between 40° and 100° by a least-square calculation after correcting 2θ with Nelson and Rieley's method [14]. Fig. 2 shows the lattice parameters of α-$Zr_{1-x}Sc_xW_2O_{8-y}$ ($x = 0$–0.04), α-$Zr_{0.96}M_{0.04}W_2O_{8-y}$ (M = In and Y) and α-$Zr_{1-x}Hf_xW_2O_8$ ($x = 0$–1) solid solutions at 121 K as a function of substituted content. The lattice parameters of α-$Zr_{1-x}Hf_xW_2O_8$ ($x = 0$–1) substituted by the same valence decrease linearly with increasing hafnium content, reflecting smaller ionic radius of hafnium (85 pm) than that of zirconium (86 pm) [15]. The dependence of the

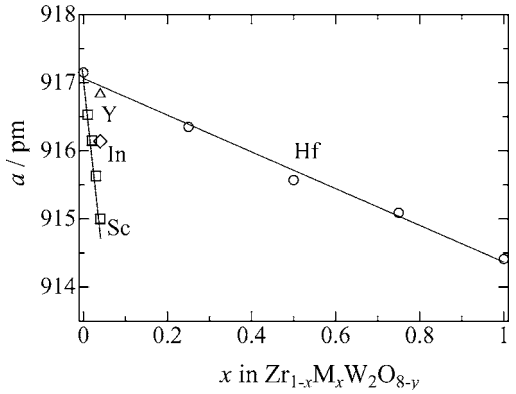

Fig. 2. Lattice parameters of (□) α-$Zr_{1-x}Sc_xW_2O_{8-y}$ (x = 0–0.04), (◇) α-$Zr_{0.96}In_{0.04}W_2O_{8-y}$, (△) α-$Zr_{0.96}Y_{0.04}W_2O_{8-y}$ and (○) α-$Zr_{1-x}Hf_xW_2O_8$ solid solutions at 121 K as a function of substituted content.

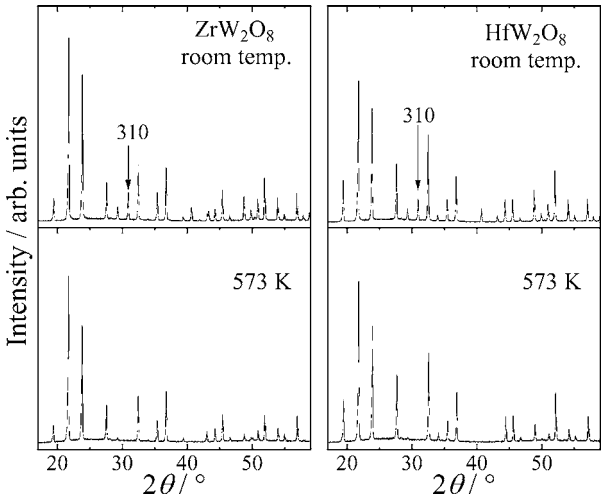

Fig. 3. Powder XRD patterns of ZrW_2O_8 and HfW_2O_8 at room temperature and 573 K.

lattice parameter on hafnium content follows the Vegard's law, and α-$Zr_{1-x}Hf_xW_2O_8$ (x = 0–1) is considered to form a complete solid solution. Closman and Sleight [8] reported that the lattice parameter of α-$ZrW_{2-x}Mo_xO_8$ substituted for W site by the same valence of Mo(VI) decreased with the increase of Mo content, due to smaller ionic radius of molybdenum (55 pm) than that of tungsten (56 pm). It can be expected that the lattice parameter of α-$Zr_{1-x}Sc_xW_2O_{8-y}$ (x = 0–0.04) substituted for zirconium site by scandium increases with increasing scandium content, because the ionic radius of Sc^{3+} (88.5 pm) is larger than that of Zr^{4+} (86 pm). However, the experimental results show the opposite tendency, although the lattice parameter of α-$Zr_{1-x}Sc_xW_2O_{8-y}$ (x = 0–0.04) linearly decreases up to $x = 0.04$ against scandium content, following the Vegard's law. One solution of this problem can be oxygen defect which was made by difference of valence of Zr^{4+} and Sc^{3+} in α-$Zr_{1-x}Sc_xW_2O_{8-y}$ to conserve electrical neutrality. The increase of lattice parameter in the order of Sc, In and Y for α-$Zr_{0.96}M_{0.04}W_2O_{8-y}$ in Fig. 2 may be explained by larger decrease of lattice parameter due to oxygen defect and smaller increase in the order of the ionic radius of substituted ions, Sc^{3+} (88.5 pm), In^{3+} (94.0 pm) and Y^{3+} (104.0 pm). It is noticed that the dependence of lattice parameter on hafnium content substituted by the same valence is smaller than that on scandium, indium and yttrium contents substituted by lower valence, where oxygen defect is formed.

3.2. α-to-β structural phase transition

3.2.1. XRD data

Fig. 3 shows the powder XRD patterns of ZrW_2O_8 and HfW_2O_8 at room temperature and 573 K. The powder XRD pattern of HfW_2O_8 at room temperature is very similar to that of ZrW_2O_8 by the previous works [2,3]. A few diffraction peaks of ZrW_2O_8 and HfW_2O_8, for example 3 1 0 peak, are absent at 573 K in comparison with the powder patterns at room temperature. The indices of the disappearing peaks in $Zr_{0.96}M_{0.04}W_2O_{8-y}$ (M = Sc, In and Y) and $Zr_{1-x}Hf_xW_2O_8$ (x = 0.25, 0.5 and 0.75) were also identical to those in ZrW_2O_8 on the α-to-β phase transition. This disappearance, thus, suggests that $Zr_{0.96}M_{0.04}W_2O_{8-y}$ (M = Sc, In and Y) and $Zr_{1-x}Hf_xW_2O_8$ (x = 0.25, 0.5 and 0.75) undergo the α-to-β phase transition above room temperature.

Fig. 4 shows the lattice parameter of $Zr_{0.96}M_{0.04}W_2O_{8-y}$ (M = Sc, In and Y) and $Zr_{0.5}Hf_{0.5}W_2O_8$ solid solutions as a function of temperature, together with that of ZrW_2O_8. An anomaly in the lattice parameter of $Zr_{0.96}M_{0.04}W_2O_{8-y}$ (M = Sc, In and Y) and $Zr_{0.5}Hf_{0.5}W_2O_8$ solid solutions is seen for each sample in the temperature range from 300 to 500 K, similar to that of ZrW_2O_8 [10]. The α-to-β phase transition temperature of $Zr_{1-x}Hf_xW_2O_8$ (x = 0 and 0.5) solid solutions was determined from disappearance of the 3 1 0 diffraction peak in Fig. 3 and from the temperature where the lattice parameter curve in the low-temperature

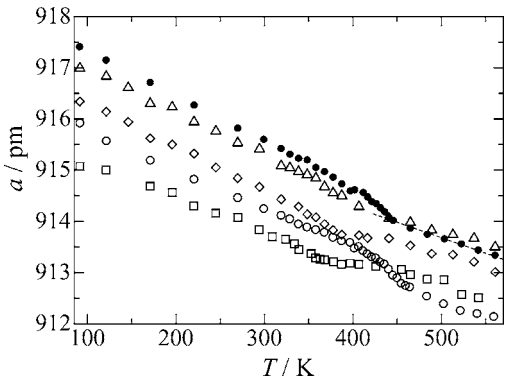

Fig. 4. Lattice parameters of (●) ZrW_2O_8, (△) $Zr_{0.96}Y_{0.04}W_2O_{8-y}$, (◇) $Zr_{0.96}In_{0.04}W_2O_{8-y}$, (□) $Zr_{0.96}Sc_{0.04}W_2O_{8-y}$ and (○) $Zr_{0.5}Hf_{0.5}W_2O_8$ as a function of temperature. A broken line in the figure is the extrapolated line of the lattice parameter in the high-temperature β-phase.

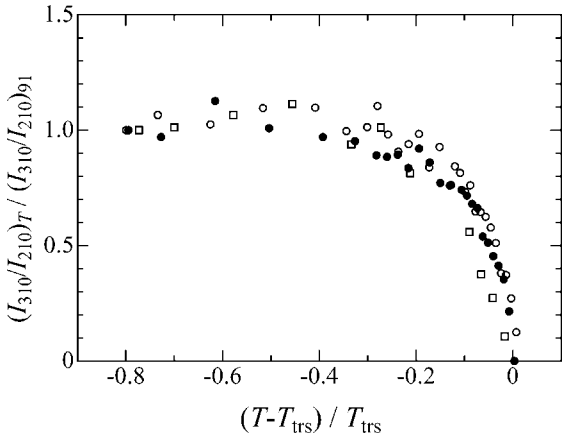

Fig. 5. Normalized intensities, $(I_{310}/I_{210})_T/(I_{310}/I_{210})_{91}$, of typical (●) ZrW_2O_8, (○) $Zr_{0.5}Hf_{0.5}W_2O_8$ and (□) $Zr_{0.98}Sc_{0.02}W_2O_{8-y}$ samples as a function of $(T - T_{trs})/T_{trs}$, where $(I_{310}/I_{210})_T$ and $(I_{310}/I_{210})_{91}$ are the relative intensities at T and 91 K, respectively.

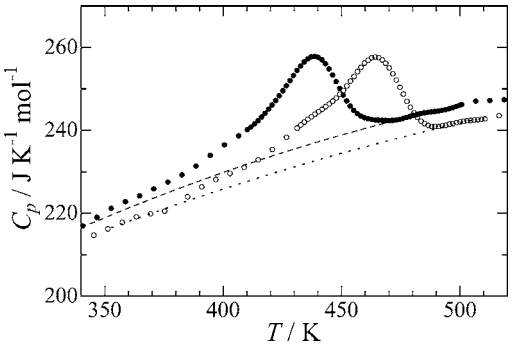

Fig. 6. Heat capacity of (●) ZrW_2O_8 and (○) HfW_2O_8 as a function of temperature. The broken and dotted lines in the figure are the base lines.

α-phase reaches the extrapolated line of the lattice parameter in the high-temperature β-phase. A typical extrapolation line of ZrW_2O_8 determined by a least-square method is shown as a broken line in Fig. 4. Phase transition temperatures (T_{trs}) of $Zr_{1-x}Hf_xW_2O_8$ ($x = 0$ and 0.5) obtained by two methods were 444 ± 2 and 456 ± 2 K, respectively. On the other hand, phase transition temperatures of $Zr_{0.96}M_{0.04}W_2O_{8-y}$ (M = Sc, In and Y) were determined to be at about 360, 380 and 390 K by the former method, respectively.

The 3 1 0 peak in Fig. 3 is considered to be one indicator in the order–disorder-type phase transition, since the 3 1 0 diffraction peak disappears above α-to-β structural phase transition temperature, where $P2_13$ in the low-temperature α-phase changes to $Pa\bar{3}$ in the high-temperature β-phase. The relative intensity of $(I_{310}/I_{210})_T$ at the temperature T and that of $(I_{310}/I_{210})_{91}$ at 91 K were calculated from XRD profiles, where I_{310} and I_{210} are intensities of 3 1 0 and 2 1 0 diffraction peaks, respectively. Fig. 5 shows normalized intensities $(I_{310}/I_{210})_T/(I_{310}/I_{210})_{91}$ of typical ZrW_2O_8, $Zr_{0.5}Hf_{0.5}W_2O_8$ and $Zr_{0.98}Sc_{0.02}W_2O_{8-y}$ samples as a function of $(T - T_{trs})/T_{trs}$, where T_{trs} is the α-to-β structural phase transition temperature. The normalized intensities of $Zr_{0.98}Sc_{0.02}W_2O_{8-y}$ and $Zr_{0.5}Hf_{0.5}W_2O_8$ follow the same curve as that of ZrW_2O_8. The normalized intensities are constant in the low-temperature region and approach to zero at T_{trs}. These facts support that $Zr_{1-x}Sc_xW_2O_{8-y}$ (x = 0–0.04) and $Zr_{1-x}Hf_xW_2O_8$ (x = 0–1) have the same phase transition mechanism as ZrW_2O_8.

3.2.2. Heat capacity data

In order to get further information on thermodynamic properties of $Zr_{1-x}Hf_xW_2O_8$ ($x = 0$, 0.5 and 1) solid solutions, a calorimetric experiment was performed from 340 to 520 K by an adiabatic scanning calorimeter. Fig. 6 shows heat capacity, C_p, of ZrW_2O_8 and HfW_2O_8 as a function of temperature by the present authors [5,10]. Curiously, the magnitude of heat capacity before and after phase transition of HfW_2O_8 is smaller than that of ZrW_2O_8, in spite of the larger mass of hafnium than zirconium. The inversion of the heat capacity may result from a difference in frequency of high-energy optical phonon modes of Zr–O and Hf–O. The lattice parameter and ionic radius suggest that the Hf–O bond is shorter and stronger than Zr–O one, leading the stretching vibration modes of Hf–O to higher energy than those of Zr–O. Therefore, the vibration modes of Hf–O probably have smaller contribution to the heat capacity than those of Zr–O at the same temperature and a more detailed discussion is given elsewhere [16]. Those facts demonstrate the inadequate statement that physical properties of two compounds are almost identical, as pointed out by Sleight and coworkers [1,2].

An anomalous peak in heat capacity of ZrW_2O_8 and HfW_2O_8 is seen at about 440 and 460 K in Fig. 6, respectively. The anomalous temperature range in the heat capacity of ZrW_2O_8 seems to correspond to that in lattice parameter in Fig. 4. The anomaly, therefore, attributes to the α-to-β structural phase transition. The shape of the anomaly of HfW_2O_8 is very similar to that of ZrW_2O_8, but the anomalous peak in heat capacity of HfW_2O_8 is 26 K higher than that of ZrW_2O_8. It is very interesting to note that, if the entire heat capacity of ZrW_2O_8 shifts to higher temperature by 26 K, the heat capacity curve of ZrW_2O_8 matches with that of HfW_2O_8. For more detailed discussion on the thermodynamic properties of the phase transition, it is necessary to separate the excess heat capacity due to the phase transition from the total heat capacity by determining the base line. In general, the base line may be determined by interpolating heat capacities in both higher- and lower-temperature ranges excluding the phase transition region. Smooth interpolating curve of ZrW_2O_8 and HfW_2O_8, as shown by the broken and dotted lines, respectively, in Fig. 6, was thus estimated for the base line of both samples to be consistent each other. The shape of the excess heat capacity for ZrW_2O_8 and HfW_2O_8 is remarkably similar to each other and regarded as λ-type, which is a general shape of the second-order phase transition. Accordingly, the phase transition of ZrW_2O_8 and HfW_2O_8 is of second (or higher) order. This is also supported by the X-ray experiment, which shows the continuous temperature

Table 1
Transition temperature (T_{trs}), excess enthalpy ($\Delta_{trs}H$) and entropy ($\Delta_{trs}S$) attributable to the phase transition of $Zr_{1-x}Hf_xW_2O_8$ (x = 0, 0.5 and 1) determined by heat capacity measurement, together with transition temperature (T_{trs}) by XRD measurement

	T_{trs} (XRD) (K)	T_{trs} (ASC) (K)	$\Delta_{trs}H$ ($J\,mol^{-1}$)	$\Delta_{trs}S$ ($J\,K^{-1}\,mol^{-1}$)
ZrW_2O_8	444 ± 2	437 ± 1	907 ± 10	2.1 ± 0.2
$Zr_{0.5}Hf_{0.5}W_2O_8$	456 ± 2	447 ± 2	924 ± 10	2.1 ± 0.2
HfW_2O_8	468 ± 2	463 ± 1	934 ± 10	2.1 ± 0.2

dependence on the lattice parameter around the phase transition temperature as seen in Fig. 4.

Transition temperature (T_{trs}), excess enthalpy ($\Delta_{trs}H$) and entropy ($\Delta_{trs}S$) attributable to the phase transition of $Zr_{1-x}Hf_xW_2O_8$ (x = 0, 0.5 and 1) were determined from heat capacity data and the results are summarized in Table 1, where transition temperature determined by X-ray diffraction method is also shown. Transition temperatures of ZrW_2O_8 and HfW_2O_8 decided from peak in the heat capacity measurement are 5–7 K lower than those determined by XRD measurement as seen in Table 1. In ASC the sample in the calorimeter vessel was in some He gas to assist quick thermal equilibration. On the other hand, the XRD measurement was carried out under vacuum environment, where the sample showed poorer thermal conductivity due to larger gas thermal resistance among particles. This different thermal conductivity of the sample in ASC and XRD measurements may lead to the difference in the phase transition temperature. The magnitudes of $\Delta_{trs}H$ and $\Delta_{trs}S$ depend on the choice of the base line, which is not included in the error assessment in Table 1. The present $\Delta_{trs}H$ and $\Delta_{trs}S$ should be regarded as the minimum enthalpy and entropy of phase transition, respectively. It is possible that a depression of the base line, which extends the temperature range for the integration of the excess heat capacity, leads to larger values of $\Delta_{trs}H$ and $\Delta_{trs}S$. The obtained $\Delta_{trs}S$ ($2.1\,J\,K^{-1}\,mol^{-1}$) of $Zr_{1-x}Hf_xW_2O_8$ (x = 0, 0.5 and 1) agrees well within the possible estimated errors. This coincidence of the excess entropy suggests that $Zr_{1-x}Hf_xW_2O_8$ (x = 0, 0.5 and 1) undergoes the phase transition with the same order–disorder mechanism.

The order–disorder α-to-β phase transition in ZrW_2O_8 results from disordering of the orientation of the two WO_4 tetrahedra (and crystallographic equivalents) that lie on the [1 1 1] body diagonal in the unit cell. Two disordering processes have been proposed so far. One is an inverting process with breaking and rebuilding the bond between terminal oxygen and tungsten ions [2,3], while the other is without breaking the bond [4]. The available space for the two WO_4 tetrahedra suggests that only two orientations can be taken into consideration in a concerted manner [2–4]. The entropy of the phase transition is thus expected to be $R\ln 2$ ($=5.8\,J\,K^{-1}\,mol^{-1}$) as a magnetic transition in a spin $\frac{1}{2}$, where R is the gas constant. On the other hand, if two tetrahedra can independently take two orientations, the expected entropy of transition is $R\ln 4$ ($=11.5\,J\,K^{-1}\,mol^{-1}$). The obtained $\Delta_{trs}S$ ($=2.1\,J\,K^{-1}\,mol^{-1}$) is even smaller than $R\ln 2$, implying that the former is preferred from the thermodynamic point of view. The smallest of $\Delta_{trs}S$ can be attributed to the overestimation of the base line. If the base line can be estimated correctly, the entropy of the α-to-β phase transition would become larger, but not exceed $R\ln 2$, because the present $\Delta_{trs}S$ is only 36% of $R\ln 2$. The magnitude of the excess entropy supports that the phase transition is of order–disorder-type, where two WO_4 tetrahedra on the [1 1 1] diagonals in the unit cell have only two conformations in a concerted manner. This suggestion is not contradictory to the previous reports [1,2] as well as the X-ray diffraction results described above. In order to determine the entropy and enthalpy of phase transition more precisely, heat capacity measurement of ZrW_2O_8 was recently carried out in the temperature range from 10 to 483 K by an adiabatic calorimeter at Research Center for Molecular Thermodynamics, Osaka University, and the heat capacity and the thermodynamic data of phase transition will be published elsewhere.

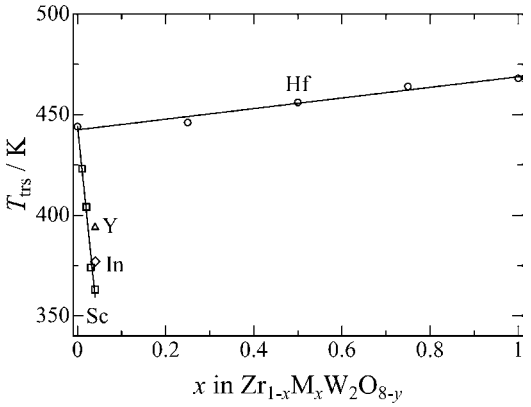

Fig. 7. Transition temperature of (□) $Zr_{1-x}Sc_xW_2O_{8-y}$ (x = 0–0.04), (◇) $Zr_{0.96}In_{0.04}W_2O_{8-y}$, (△) $Zr_{0.96}Y_{0.04}W_2O_{8-y}$ and (○) $Zr_{1-x}Hf_xW_2O_8$ determined by XRD measurement as a function of substituted content.

3.2.3. Effect of substituted ions and its content on phase transition temperature

Fig. 7 shows phase transition temperatures of $Zr_{1-x}Sc_xW_2O_{8-y}$ (x = 0–0.04), $Zr_{0.96}M_{0.04}W_2O_{8-y}$ (M = In and Y) and $Zr_{1-x}Hf_xW_2O_8$ (x = 0–1) as a function of substituted content. The phase transition temperature of $Zr_{1-x}Hf_xW_2O_8$ (x = 0–1) solid solutions substituted for zirconium site by the same valence increases with increasing hafnium content, and enthalpy of transition $\Delta_{trs}H$ also increases as seen in Table 1. This means that the energy necessary for the order–disorder phase transition is larger and the transition temperature is higher. On the other hand, phase transition temperature of $Zr_{0.96}M_{0.04}W_2O_{8-y}$ (M = Sc, In and Y) substituted by lower valence decreased drastically, probably due to oxygen defect, compared to that of $Zr_{1-x}Hf_xW_2O_8$ substituted by the same valence. This fact

can be explained by the decrease in the degree of ordering, corresponding to intensity ratio $(I_{3\,1\,0}/I_{2\,1\,0})_{121}$ which is one indicator of the order parameters, since the intensity ratio $(I_{3\,1\,0}/I_{2\,1\,0})_{121}$ of $Zr_{0.96}M_{0.04}W_2O_{8-y}$ (M = Sc, In and Y) in α-phase is about half of that of $Zr_{0.5}Hf_{0.5}W_2O_8$ and ZrW_2O_8 as seen in Fig. 1. The same trend is reported for $ZrW_{2-x}Mo_xO_8$, where the disordering of $ZrW_{2-x}Mo_xO_8$ in α-phase is larger than that of ZrW_2O_8 and the transition temperature of the former is lower than that of the latter [8]. It is needed to get more precise information on the intensity ratio $(I_{3\,1\,0}/I_{2\,1\,0})_{121}$ of $Zr_{0.96}M_{0.04}W_2O_{8-y}$ (M = Sc, In and Y) in order to discuss the tendency of ionic size of substituted ion and its content. It is interesting to note that the lattice parameter of $Zr_{0.96}M_{0.04}W_2O_{8-y}$ (M = Sc, In and Y) in Fig. 2 and their transition temperature in Fig. 7 as a function of substituted content show the similar tendency.

4. Conclusions

(1) Lattice parameters of α-$Zr_{1-x}Hf_xW_2O_8$ and α-$ZrW_{2-x}Mo_xO_8$ substituted by the same valence decreased with substituted content, due to smaller ionic radius of substituted ion than host lattice.

(2) Lattice parameter of α-$Zr_{1-x}Sc_xW_2O_{8-y}$ substituted by lower valence decreased with substituted content, probably due to oxygen defect. The increase of lattice parameter for α-$Zr_{0.96}M_{0.04}W_2O_{8-y}$ (M = Sc, In and Y) in the order of Sc, In and Y can be explained by large decrease of lattice parameter due to oxygen defect and smaller increase due to ionic radius of host and substituted ions.

(3) The entropy of α-to-β structural phase transition in $Zr_{1-x}Hf_xW_2O_8$ (x = 0, 0.5 and 1) has the same value of $2.1\,J\,K^{-1}\,mol^{-1}$ and the normalized 3 1 0 diffraction peaks of $Zr_{1-x}Hf_xW_2O_8$ (x = 0 and 0.5), and $Zr_{0.98}Sc_{0.02}W_2O_{8-y}$ as one indicator of the order parameters follow the universal curve against $(T-T_{trs})/T_{trs}$. These results support that $Zr_{1-x}Hf_xW_2O_8$ and $Zr_{1-x}Sc_xW_2O_{8-y}$ have the same order–disorder phase transition mechanism.

(4) The abrupt decrease in phase transition temperature of $Zr_{1-x}M_xW_2O_{8-y}$ (M = Sc, In and Y), in comparison with that of $Zr_{1-x}Hf_xW_2O_8$, can be caused by the decrease of ordering in the α-phase due to oxygen defect.

References

[1] T.A. Mary, J.S.O. Evans, T. Vogt, A.W. Sleight, Science 272 (1996) 90.
[2] J.S.O. Evans, T.A. Mary, T. Vogt, M.A. Subramanian, A.W. Sleight, Chem. Mater. 8 (1996) 2809.
[3] J.S.O. Evans, W.I.F. David, A.W. Sleight, Acta Crystallogr. B 55 (1999) 333.
[4] A.K.A. Pryde, K.D. Hammonds, M.T. Dove, V. Heine, J.D. Gale, M.C. Warren, Phase Transit. 61 (1997) 141.
[5] Y. Yamamura, N. Nakajima, T. Tsuji, Solid State Commun. 114 (2000) 453.
[6] A.W. Sleight, T.A. Mary, J.S.O. Evans, US Patent 5 514 360 (1995).
[7] N. Nakajima, Y. Yamamura, T. Tsuji, J. Therm. Anal., 70 (2002) 337.
[8] C. Closman, A.W. Sleight, J. Solid State Chem. 139 (1998) 424.
[9] J.S.O. Evans, P.A. Hanson, R.M. Ibberson, N. Duan, U. Kameswari, A.W. Sleight, J. Am. Chem. Soc. 122 (2000) 8694.
[10] Y. Yamamura, N. Nakajima, T. Tsuji, Phys. Rev. B 64 (2001) 184109.
[11] K. Naito, N. Kamegashira, N. Yamada, J. Kitagawa, J. Phys. E: Sci. Instrum. 6 (1973) 836.
[12] K. Naito, H. Inaba, M. Ishida, Y. Saito, H. Arima, J. Phys. E: Sci. Instrum. 7 (1974) 464.
[13] D.G. Archer, J. Phys. Chem. Ref. Data 22 (1993) 1441.
[14] J.B. Nelson, D.P. Riley, Proc. Phys. Soc. London 57 (1945) 160.
[15] R.D. Shannon, Acta Crystallogr. Sect. A: Cryst. Phys. Diffr. Theor. Gen. Crystallogr. A 32 (1976) 751.
[16] Y. Yamamura, N. Nakajima, T. Tsuji, K. Saito, M. Sorai, Phys. Rev. B 66 (2002) 014301.